

## Boundary-layer convection and diurnal variation of vertical-velocity characteristics in the free troposphere

By ANDREAS MUSCHINSKI<sup>1\*</sup>, PHILLIP B. CHILSON<sup>2</sup>, ROBERT D. PALMER<sup>3</sup>, DAVID A. HOOPER<sup>2</sup>, GERHARD SCHMIDT<sup>4</sup> and HANS STEINHAGEN<sup>5</sup>

<sup>1</sup>*CIRES and NOAA Environmental Technology Laboratory, USA*

<sup>2</sup>*Swedish Institute of Space Physics, Sweden*

<sup>3</sup>*University of Nebraska, USA*

<sup>4</sup>*Max-Planck-Institut für Aeronomie, Germany*

<sup>5</sup>*Deutscher Wetterdienst, Meteorologisches Observatorium Lindenberg, Germany*

(Received 21 February 2000; revised 1 September 2000)

### SUMMARY

During the field experiment SOMARE-99 (Sounding System Multifrequency Atmospheric Radar Experiment 1999), the troposphere above the Harz Mountains in Northern Germany was observed with the SOUSY VHF radar, with four microbarographs, and with 26 radiosondes launched every 3 h from nearby the radar site. This paper examines the 72 h period between 0000 UTC 25 May and 0000 UTC 28 May. Time series, root-mean-square values, and power spectra of radar-observed vertical-wind,  $w$ , fluctuations in the free troposphere and of pressure,  $p$ , fluctuations at the surface are presented and discussed. A pronounced diurnal cycle was observed: standard deviations (from 1 h periods) were about  $10 \text{ cm s}^{-1}$  ( $w$ ) and  $2 \text{ Pa}$  ( $p$ ) at night and up to  $60 \text{ cm s}^{-1}$  and  $6 \text{ Pa}$  during daytime. This is seen as evidence for the relevance of boundary-layer convection for short-period gravity waves in the free troposphere. Frequency spectra of  $w$  show a power-law drop-off beyond the Brunt–Väisälä frequency with logarithmic slopes close to  $-5/3$  at moderate and strong wind speeds and down to  $-3$  or  $-4$  at weak winds (smaller than  $5 \text{ m s}^{-1}$ ), supporting earlier work on the effects of Doppler shift on Eulerian gravity-wave spectra. The  $w$  spectra, which have been calculated from 8 h long  $w$  time series (sampling period 1 min), have a noise floor of  $10^{-3} \text{ m}^2 \text{ s}^{-2} \text{ Hz}^{-1}$  or less. This corresponds to an uncorrelated noise with a standard deviation of  $3 \text{ mm s}^{-1}$  for the 1 min samples. The concept of *gravity-wave intermittency* is introduced, in analogy to a well-established concept in turbulence physics. It is demonstrated how this concept can be used to distinguish turbulence from gravity waves empirically.

KEYWORDS: Convection Gravity waves Vertical-wind spectra VHF radars

### 1. INTRODUCTION

Turbulence and gravity waves are two important types of atmospheric motion at microscales and mesoscales. The classical picture of turbulence is that of three-dimensional, statistically isotropic, random motion (e.g. Kolmogorov 1941; Batchelor 1953; Lumley and Panofsky 1964). The classical picture of gravity-wave motion, however, is that of primarily vertical, oscillatory motion (Brunt 1927). While buoyancy forces suppress turbulence in the stably stratified atmosphere, buoyancy forces are essential for the occurrence of gravity waves. The physical nature of turbulence is diffusive, while the nature of gravity-wave motion is propagative.

A convenient property of turbulent motion is its universality (Kolmogorov 1941; Batchelor 1953). The universality of turbulence characteristics has been theoretically predicted and experimentally verified in the atmospheric surface layer (e.g. Monin and Obukhov 1953, 1954; Kaimal *et al.* 1972) and in the convective boundary layer (e.g. Obukhov 1960; Kaimal *et al.* 1976). Often, gravity waves are not monochromatic, which suggests a statistical approach. A theoretical framework for universal gravity-wave spectra in the ocean was put forward by Garrett and Munk (1972, 1975). VanZandt (1982) suggested application of the Garrett–Munk model for atmospheric gravity waves.

If the mean velocity is sufficiently large compared with the magnitude of the turbulent velocity fluctuations, frequency spectra of fully developed turbulence advected

\* Corresponding author: Cooperative Institute for Research in Environmental Sciences (CIRES), University of Colorado, and NOAA Environmental Technology Laboratory, Boulder, 325 Broadway, R/ET2, Colorado 80305-3328, USA. e-mail: Andreas.Muschinski@noaa.gov

with a mean velocity  $V$  past a sensor show a  $f^{-5/3}$  frequency spectrum that can be mapped unambiguously via Taylor's (1938) frozen turbulence hypothesis into a one-dimensional (streamwise)  $k^{-5/3}$  wave-number spectrum. Because this mapping is unambiguous and since turbulence spectra are universal in wave-number space, the measured frequency spectra of turbulence enable turbulence structure parameters to be retrieved unambiguously.

The mapping of an *intrinsic*, Lagrangian gravity-wave spectrum into an *apparent*, Eulerian frequency spectrum that is measured by a ground-based observer has been analytically investigated by Sheffler and Liu (1985, 1986). This mapping has been called *Doppler shift*. Further analytical and numerical examination of Doppler-shifted gravity-wave spectra has been done by Fritts and VanZandt (1987) and VanZandt *et al.* (1991). Universality can be expected only for the intrinsic gravity-wave spectrum. Because the inverse mapping of an observed gravity-wave frequency spectrum into an intrinsic gravity-wave spectrum is usually not possible owing to ambiguities, and because the algebraic form of the intrinsic gravity-wave spectrum cannot be derived from first principles (VanZandt *et al.* 1991), the interpretation of Eulerian gravity-wave spectra is much more complicated than the interpretation of Eulerian turbulence spectra.

Gravity waves often carry large vertical fluxes of horizontal momentum, thereby connecting with each other the tendencies of the horizontal wind vector at different altitudes. Through coupling the momentum budgets of the troposphere, the stratosphere, and even the mesosphere, gravity waves are key to the understanding of the momentum budget of the atmosphere (e.g. Hines 1960; Gossard 1962; Hines and Reddy 1967; Lindzen 1981; Nastrom *et al.* 1985). Various phenomena can lead to the generation of gravity waves in the troposphere (Gossard and Hooke, 1975 pp. 359 ff.; Einaudi *et al.* 1979): flow over mountains (e.g. Scorer 1949; Balsley and Carter 1989; Lilly 1971; Hines 1989; Ralph *et al.* 1992; Worthington 1996, 1998; Zhou *et al.* 1996; Ralph *et al.* 1997; Worthington *et al.* 2001); upper-tropospheric jet streams (e.g. Herron and Tolstoy 1969; Neisser 1985); and boundary-layer convection (Townsend 1966; Nastrom and Gage 1984; Clark *et al.* 1986; Kuettner *et al.* 1987; Hauf and Clark 1989; Hauf 1993).

This case-study relies on observations obtained during Sounding System Multifrequency Atmospheric Radar Experiment 1999 (SOMARE-99) in the Harz mountains in Northern Germany. The main purpose of SOMARE-99 was to demonstrate the feasibility of the range imaging (RIM) technique (Palmer *et al.* 1999) for the observation of thin scattering layers in the troposphere. During SOMARE-99, RIM was implemented for the first time on an atmospheric radar. An overview of the experiment, including the first comparison of radiosonde observations and RIM observations of scattering layers, is given by Chilson *et al.* (2001). Palmer *et al.* (2001) describes the RIM data processing and presents details of the tropospheric fine structure observed with RIM.

Here we investigate the behaviour of short-term (from one minute to several hours) variations of vertical velocity  $w$  and surface pressure  $p$  during the 72 h period between 0000 UTC 25 May and 0000 UTC 28 May. A pronounced diurnal cycle in 1 h standard deviations and in the frequency spectra of  $w$  (at altitudes from 2.7–8.7 km MSL\*) and of  $p$  is seen as evidence for the relevance of boundary-layer convection for free-tropospheric gravity-wave activity.

The variability of statistical gravity-wave parameters at relatively short time-scales is conceptually similar to the variability of the energy dissipation rate in turbulence physics, which is known as *intermittency* (e.g. Mahrt 1989). In analogy to turbulence intermittency, we introduce the concept of *gravity-wave intermittency*. It is demonstrated

\* Above mean sea level.

how this concept can be used to empirically distinguish between turbulence and gravity waves.

## 2. INSTRUMENTATION AND DATA PROCESSING

### (a) Instrumentation

The week-long field experiment SOMARE-99 was performed in May 1999 in the environment of the SOUSY VHF Radar, which is situated near Bad Lauterberg in the Harz Mountains in Northern Germany. Instrumentation consisted of the SOUSY (Sounding System) VHF radar, four microbarographs, and 26 radiosondes. The overall experimental set-up is described by Chilson *et al.* (2001).

During SOMARE-99, RIM technique (Palmer *et al.* 1999, 2001) was implemented for the first time on an atmospheric radar. The purpose and advantage of RIM over the standard Doppler technique is to overcome, at least partially, the range resolution limitations that are common in radar wind profiling by post-synthesizing the range-weighting function on the basis of frequency diversity. Another technique that makes use of frequency diversity is frequency-domain interferometry (FDI); see Kudeki and Stitt (1987). After implementation of FDI capability on the SOUSY VHF radar (Chilson and Schmidt 1996), this radar was used for the first FDI observations of upper-level Kelvin–Helmholtz billows (Chilson *et al.* 1997) and for the first FDI observations of synoptic-scale subsidence in the troposphere (Muschinski *et al.* 1999a). The main purpose of SOMARE-99 was to demonstrate the advantages of RIM over FDI.

During SOMARE-99, the SOUSY VHF radar was operated at four carrier frequencies: 53.250, 53.333, 53.583 and 53.750 MHz. The radar was operated in a vertically oriented RIM mode most of the time. For each dwell time (56 s), 512 complex signal samples were obtained by cycling through the four carrier frequencies, which resulted in one 128-point signal time series for each of the four frequencies. In another recent experiment, using the Middle and Upper Atmosphere (MU) Radar in Japan, Luce *et al.* (2001) also used four frequencies, but instead of cycling through the four frequencies during the same dwell time, they switched only between two frequencies during a single dwell time (30 s). In a sequence of three such dwell times, resulting in a total dwell time of 90 s, they cycled through three frequency pairs ( $f_2, f_3$ ), ( $f_1, f_3$ ), and ( $f_1, f_4$ ). The Luce *et al.* (2001) implementation was necessary due to limitations in the MU radar at that time and did not permit full utilization of RIM's capabilities. In the Luce *et al.* (2001) implementation, it was not possible to simultaneously synthesize signal time series for 'sub-gates' within the conventional range gates, nor was it possible to generate simultaneous but statistically independent power spectra for each of the four frequencies and for each conventional range gate.

Every 16 min the radar performed a sequence of standard (single-frequency) soundings in five beam directions: vertical and  $7^\circ$  off vertical in the four cardinal directions.

The surface pressure  $p$  at the radar site was measured with a microbarograph. Of the four pressure time series, this is the only one that we examine in this paper.

### (b) Data processing

In this study we took advantage of having four radar signals independent in frequency (and therefore four independent Doppler spectra) for each dwell time and each range gate in order to reduce the noise in the  $w$  time series. Palmer *et al.* (2001) and Chilson *et al.* (2001) demonstrate how these independent samples are used for increased range resolution. By using the median of the four independent Doppler shifts (obtained by Fourier processing using a Hanning window; see Palmer *et al.* 2001), outliers were

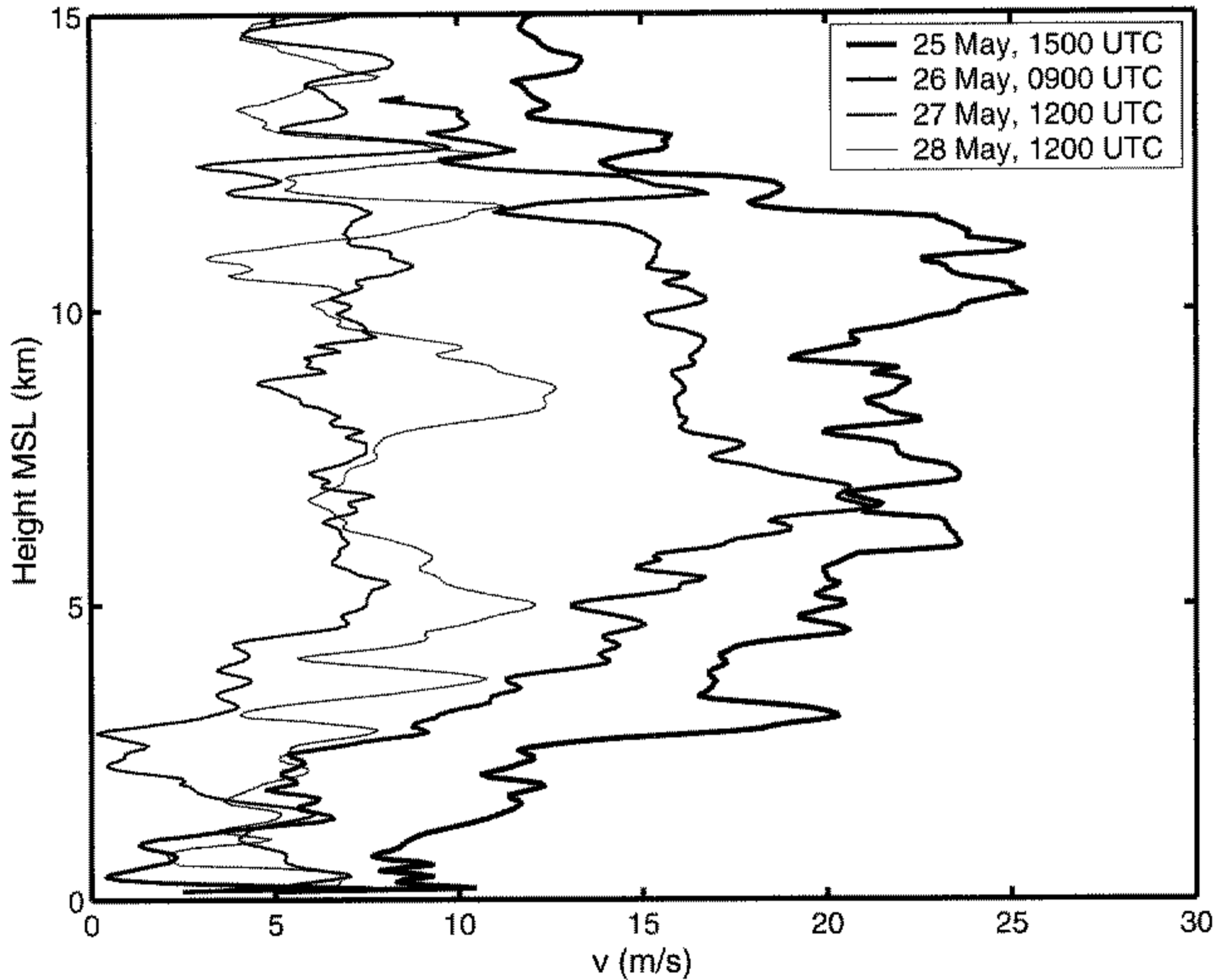


Figure 1. Vertical profiles of the horizontal wind speed, observed with radiosondes during the period from 1200 UTC 25 May to 1200 UTC 28 May 1999. Height is relative to mean sea level.

removed. Simultaneously the estimation error was reduced, because each of the four frequencies sees a different realization of phases within the same resolution volume, which leads to a different realization of the Doppler spectrum (see, e.g. Muschinski *et al.* 1999b).

Then the 56 s median  $w$  values were linearly interpolated to a 1 min grid to synchronize the radar  $w$  estimates with the surface-pressure data at the radar site, which were sampled at 60 s. The short data gaps during the off-vertical measurements were filled with values obtained by linear interpolation of  $w$  before and after the gaps.

Spectra of  $w$  and  $p$  were computed with a fast Fourier transformation (after the respective linear trend in the  $p$  time series had been removed) with no tapering in the time domain. That is, a simple box-car window was applied. Then the properly normalized raw power spectra were smoothed in the frequency domain by block averaging over logarithmically equidistant frequency bins (see, e.g. Kaimal 1986).

### 3. OBSERVATIONS

#### (a) Synoptic situation during SOMARE-99

The synoptic situation during the period 25–27 May was characterized by an upper-level Icelandic low and generally anticyclonic flow in Northern Germany. On 25 May around noon, an upper-level trough associated with the Icelandic low moved over Northern Germany to the east causing relatively high wind speeds of up to  $30 \text{ m s}^{-1}$  in the upper troposphere above the radar site on that day. After the trough had moved

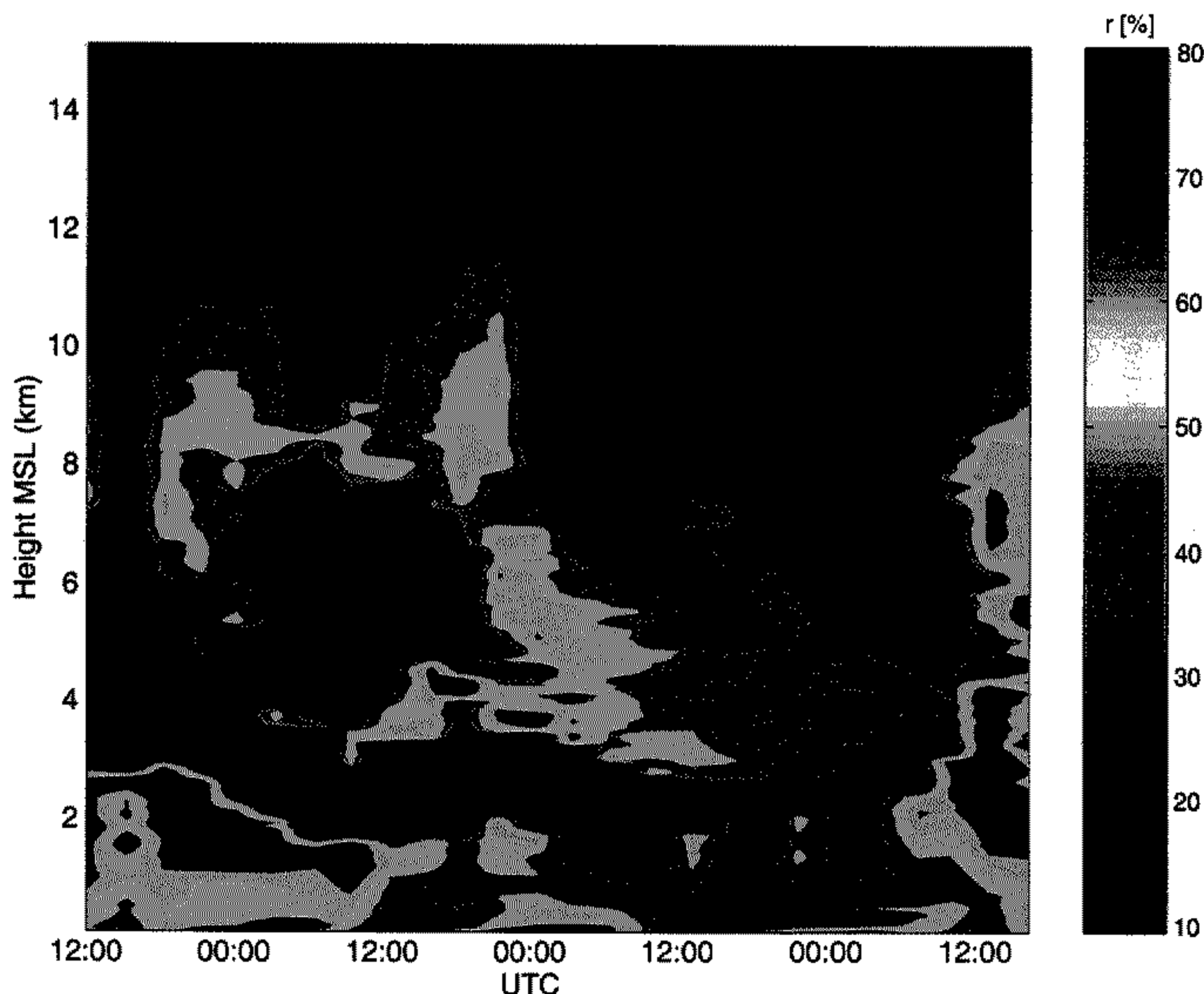


Figure 2. Time–height cross-section of relative humidity, observed with radiosondes during the period from 1200 UTC 25 May to 1200 UTC 28 May 1999. Height is relative to mean sea level.

east, wind speed throughout the troposphere decreased to  $10 \text{ m s}^{-1}$  and less. About 1000 km north of the radar site (at the latitude of Scotland), however, the polar-front jet stream was present during the entire period, which may be relevant for the generation of the horizontally propagating gravity waves observed during SOMARE-99 (e.g. Herron and Tolstoy 1969).

Figure 1 shows four vertical profiles of the horizontal wind speed measured with radiosondes around noon on 25, 26, 27 and 28 May. During this period, the wind speeds in the troposphere decreased from about  $25 \text{ m s}^{-1}$  (25 May) to  $10 \text{ m s}^{-1}$  and less (27 and 28 May).

Figure 2 is a height–time cross-section of the relative humidity. Except for 27 May, a dry region in the lower troposphere separates the moist boundary layer from the middle and upper troposphere, where the relative humidity is also generally higher than in that dry region. The boundary-layer height reached about 3 km MSL on 25 May, i.e. during the passage of the upper-level trough. During the next three days the meteorological situation was characterized by high pressure and large-scale subsidence. The subsidence resulted in lower boundary-layer inversion heights and in a less humid boundary layer on 26 and 27 May. The upper boundary of the dry region descended from about 3.5 km MSL at 0000 UTC 26 May to about 2.5 km at 0000 UTC 28 May, corresponding to a vertical velocity of about  $0.6 \text{ cm s}^{-1}$ , where this apparent vertical velocity may be due to both true vertical motion (subsidence) and horizontal advection of synoptic- or subsynoptic-scale, tilted air-mass boundaries. From observations and numerical

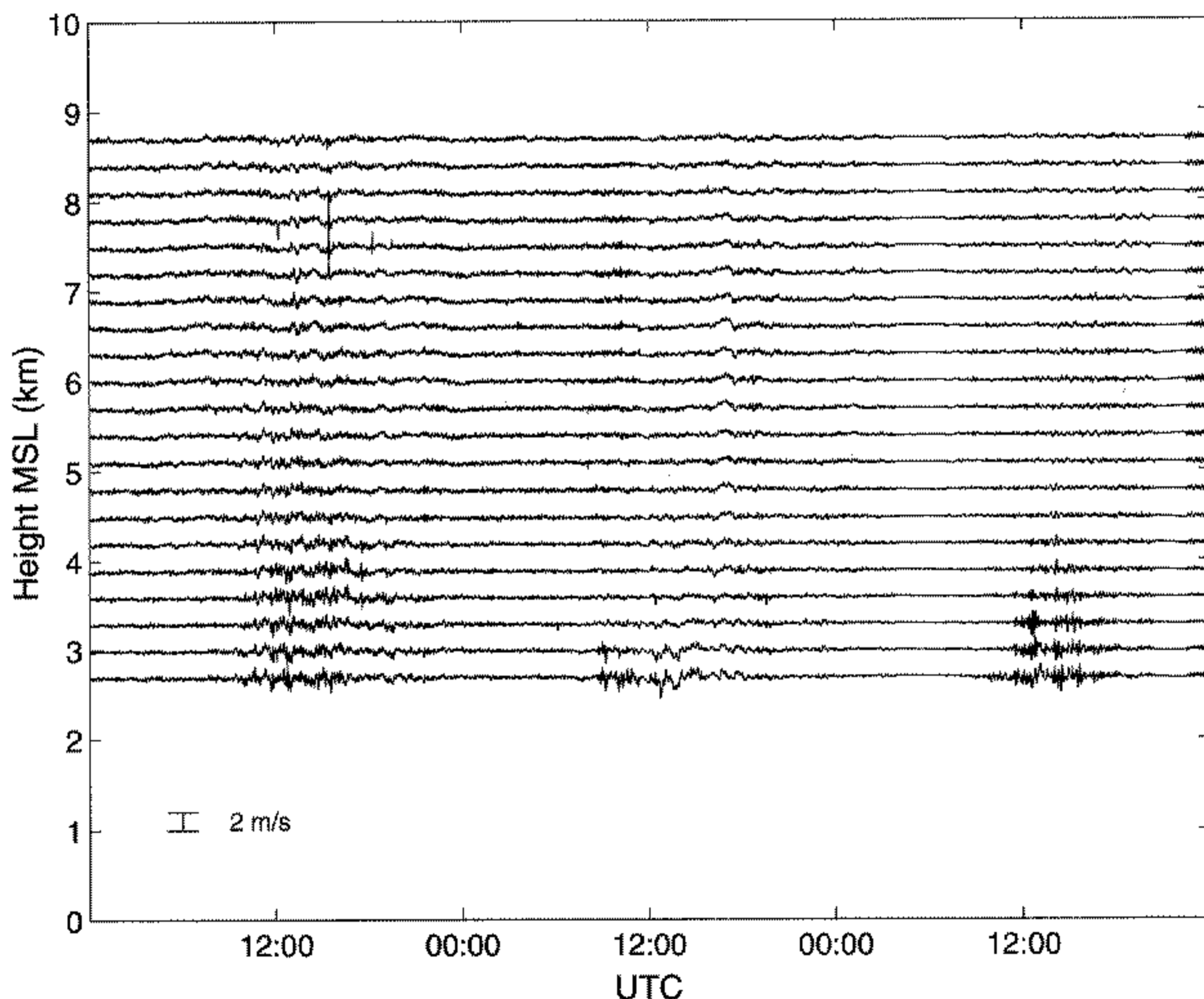


Figure 3. Vertical velocities  $w$  observed with the SOUSY VHF radar. The temporal resolution is 1 min. Note the enhanced amplitudes of the  $w$  fluctuations between about 1000 UTC and about 1800 UTC on each of 25, 26 and 27 May. Height is relative to mean sea level.

weather-forecasting data during an earlier field experiment in a similar meteorological situation, Muschinski *et al.* (1999a) obtained values up to a few centimetres per second for the true large-scale vertical velocity in the lower troposphere.

(b) *Overview: Vertical-wind fluctuations and surface-pressure fluctuations*

Vertical velocities observed with the SOUSY VHF radar during the period from 0000 UTC 25 May to 0000 UTC 28 May are shown in Fig. 3 as a staggered time series. Obviously, there is a diurnal cycle of the amplitudes of the  $w$  fluctuations. The  $w$  amplitudes are enhanced during the period from about 1000–1800 UTC on each of the three days. This diurnal cycle is most pronounced at altitudes below about 4 km but, as we show later, it is observed up to the highest observation level, which is at 8.7 km MSL.

In Fig. 4(a), the surface-pressure variations at the radar site are plotted together with the  $w$  variations at 2.7 km MSL. Figure 4(b) shows the hourly standard deviations of  $p$  ( $\sigma_p$ ) and  $w$  ( $\sigma_w$ ). Before computing the  $\sigma_p$  values, the linear trend in  $p$  was removed for each 1 h interval.

The mean value of 979.7 hPa was subtracted from the pressure values. The pressure variations shown in Fig. 4(a) are typical for a valley site during a period that is characterized by solar heating during the day and radiative cooling at night. During the night, the bottom of the valley fills up with cold air. This is associated with an increase in the mass of the air column above the valley bottom and therefore with an increase in the surface pressure in the valley. After sunrise, the air in the valley is heated and

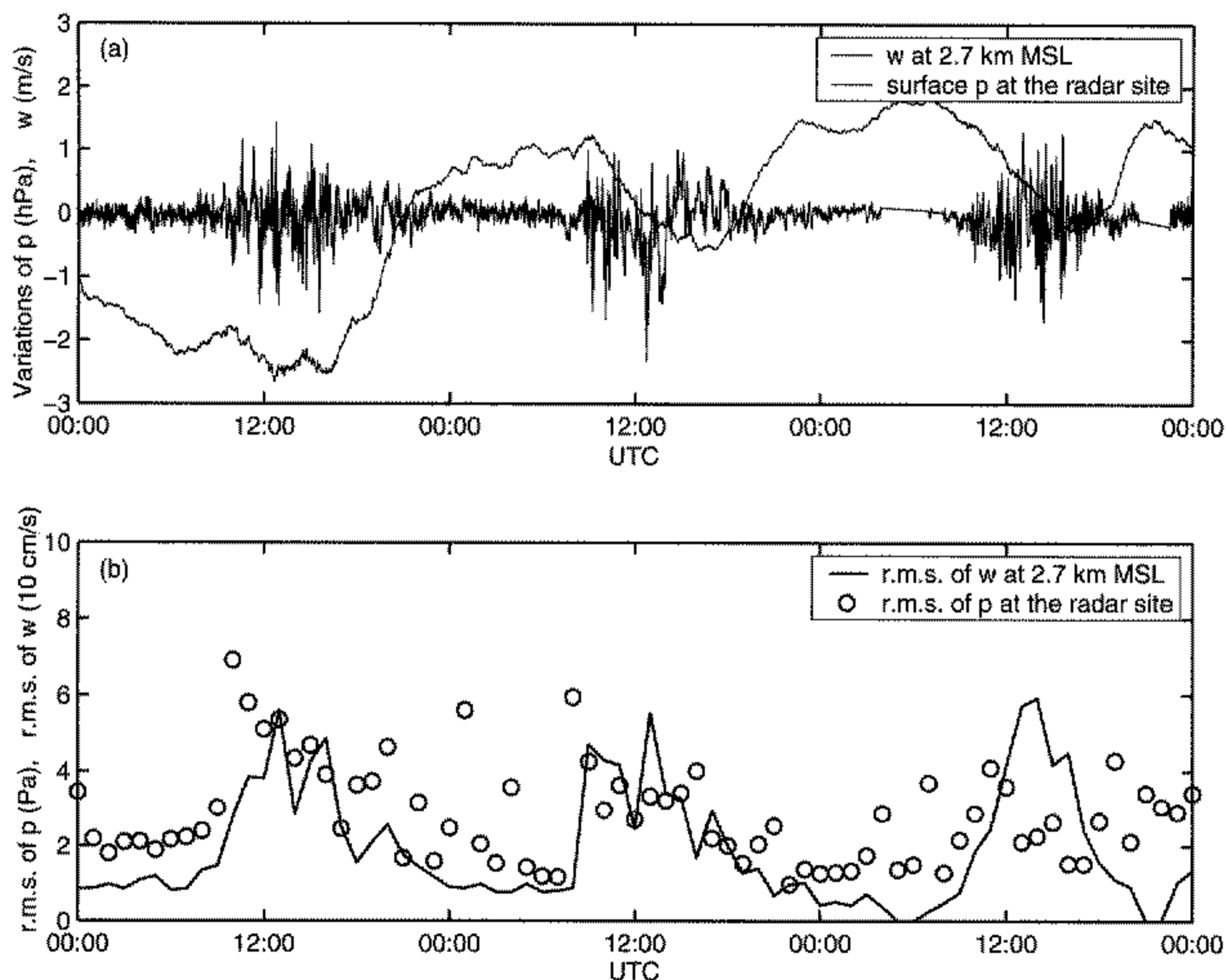


Figure 4. (a) Time series of the surface pressure  $p$  at the site of the SOUSY VHF radar (333 m) and of the vertical velocity observed at the lowest radar observation height, which is centred at 2.7 km. Height is relative to mean sea level. (b) Time series of 1 h standard deviations of  $p$  and  $w$ .

the isosurfaces of the air pressure close to the surface move downwards, which leads to a decrease of the surface pressure. That is, the surface pressure decreases during the day and increases during the night, which can be clearly seen in Fig. 4(a). Moreover, Fig. 4(a) shows that the  $w$  fluctuations at 2.7 km MSL are enhanced during daytime, i.e. during the period of decreasing surface pressure at the radar site.

Figure 4(b) shows that both  $\sigma_p$  at the surface and  $\sigma_w$  at 2.7 km MSL have maximum values during the day and minimum values at night. The maxima of  $\sigma_p$  reach 6 Pa; the maxima of  $\sigma_w$  are at  $50 \text{ cm s}^{-1}$ . During the night,  $\sigma_p$  and  $\sigma_w$  decrease to 1 Pa and  $10 \text{ cm s}^{-1}$ , respectively.

On 25 and 26 May, both  $\sigma_p$  and  $\sigma_w$  increase suddenly, i.e. within 1 h or less, at sunrise. Between afternoon and the next day's sunrise, both  $\sigma_p$  and  $\sigma_w$  decrease gradually. On 27 May, however, both  $\sigma_p$  and  $\sigma_w$  behave differently. First, the time series of  $\sigma_p$  and  $\sigma_w$  are nearly symmetric about local noon (1320 UTC); second, there is no obvious correlation between  $\sigma_p$  and  $\sigma_w$  on 27 May. We will return to the difference between 25/26 May and 27 May when we discuss the frequency spectra of  $w$  for various 8 h long periods within the 72 h long period.

Figure 5 shows a frequency spectrum of surface-pressure fluctuations,  $S_{pp}(f)$ , and four frequency spectra of  $w$  fluctuations,  $S_{ww}(f)$ . All spectra have been computed on the basis of 1 min time series obtained during the 72 h long observation period between 0000 UTC 25 May and 0000 UTC 28 May. The four  $w$  spectra correspond to  $w$  data obtained at the four lowest range gates (2.7, 3.0, 3.3 and 3.6 km MSL).

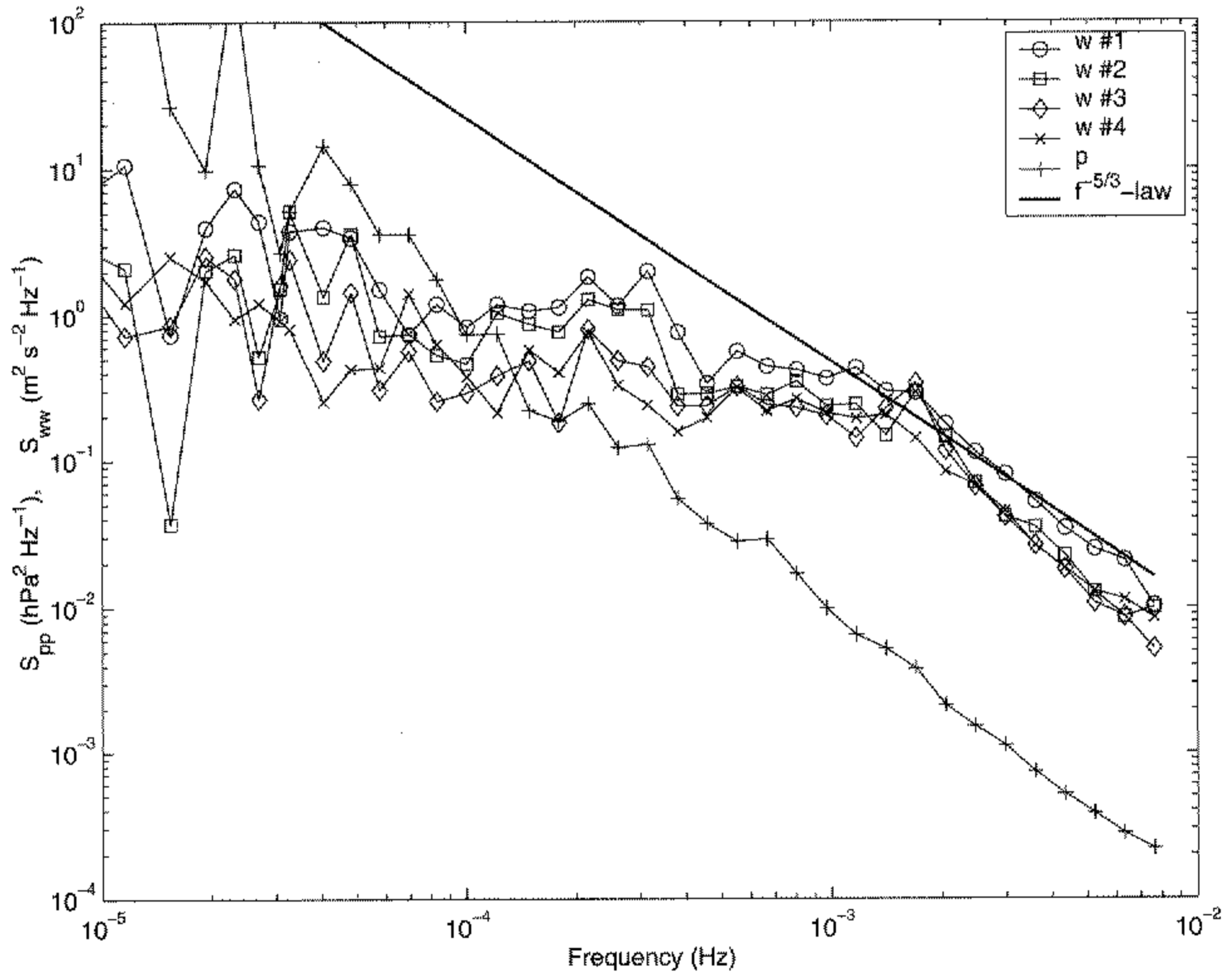


Figure 5. Frequency spectra of vertical velocity  $w$  at the lowest four range gates (centred at 2.7, 3.0, 3.3 and 3.6 km, respectively, with height relative to mean sea level), and of surface pressure  $p$  at the radar site. The spectra were computed from the time series covering the period from 0000 UTC 25 May to 0000 UTC 28 May. The  $-5/3$  power law (see text) is also shown.

The four  $S_{ww}(f)$  graphs show a behaviour similar to the spectra that Ecklund *et al.* (1985) found characteristic for 'quiet' periods: a nearly constant energy density up to the Brunt–Väisälä frequency  $1/T_{BV}$  and a drop-off at larger frequencies. The  $w$  spectra in Fig. 5 show a power-law behaviour beyond  $2 \times 10^{-3}$  Hz. Their drop-off is slightly steeper than a  $f^{-5/3}$  law. In contrast to the  $w$  spectra, the  $p$  spectrum shows the power-law behaviour down to frequencies much smaller than  $1/T_{BV}$ . The  $w$  spectra at the three lowest range gates have a local maximum at  $1.6 \times 10^{-3}$  Hz, corresponding to a period of 10.5 min, which is close to the  $T_{BV}$  of the standard atmosphere. At the fourth range gate (3.6 km MSL), the maximum of  $S_{ww}(f)$  appears at a slightly smaller frequency, indicating a slightly smaller static stability at that altitude than below.

At frequencies higher than  $5 \times 10^{-4}$  Hz (periods shorter than about 30 min), the  $S_{ww}(f)$  at range gates 2, 3 and 4 are very similar to each other but the level of  $S_{ww}(f)$  at the lowest range gate is a factor of two larger.

### (c) Spectra from six 8 h periods

Since the  $w$  and  $p$  fluctuations show a pronounced diurnal cycle during the 72 h period (Figs. 3 and 4), it is appropriate to divide the 72 h period into shorter periods and to investigate the spectral characteristics of the  $p$  and  $w$  fluctuations during these shorter periods. After inspecting the data, we selected six periods: three 8 h long early-morning



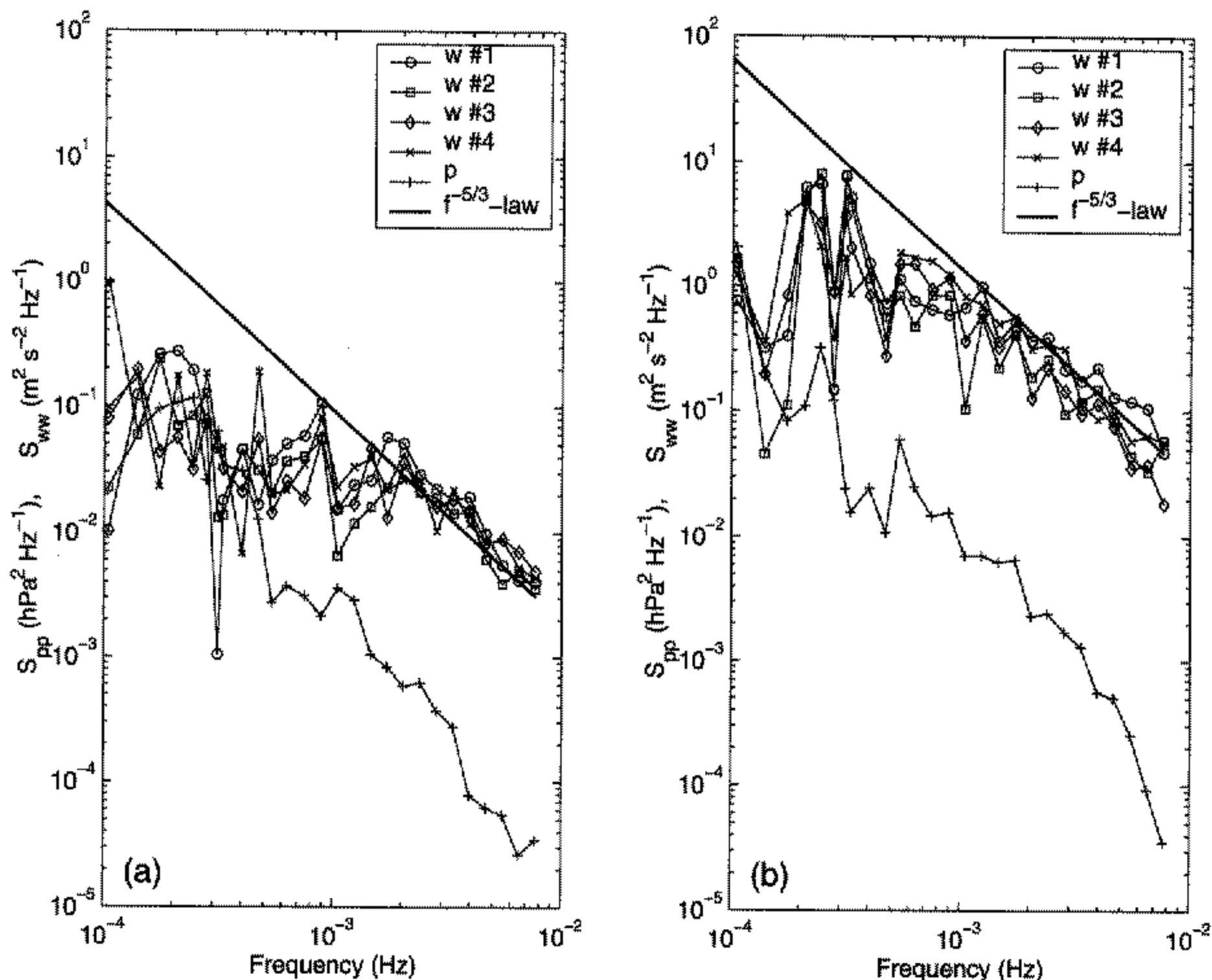


Figure 6. Frequency spectra of vertical velocity  $w$  at the lowest four range gates (centred at 2.7, 3.0, 3.3 and at 3.6 km, respectively, with height relative to mean sea level), and of surface pressure  $p$  at the radar site: (a) morning of 25 May 1999, and (b) afternoon of same day. The  $-5/3$  power law (see text) is also shown.

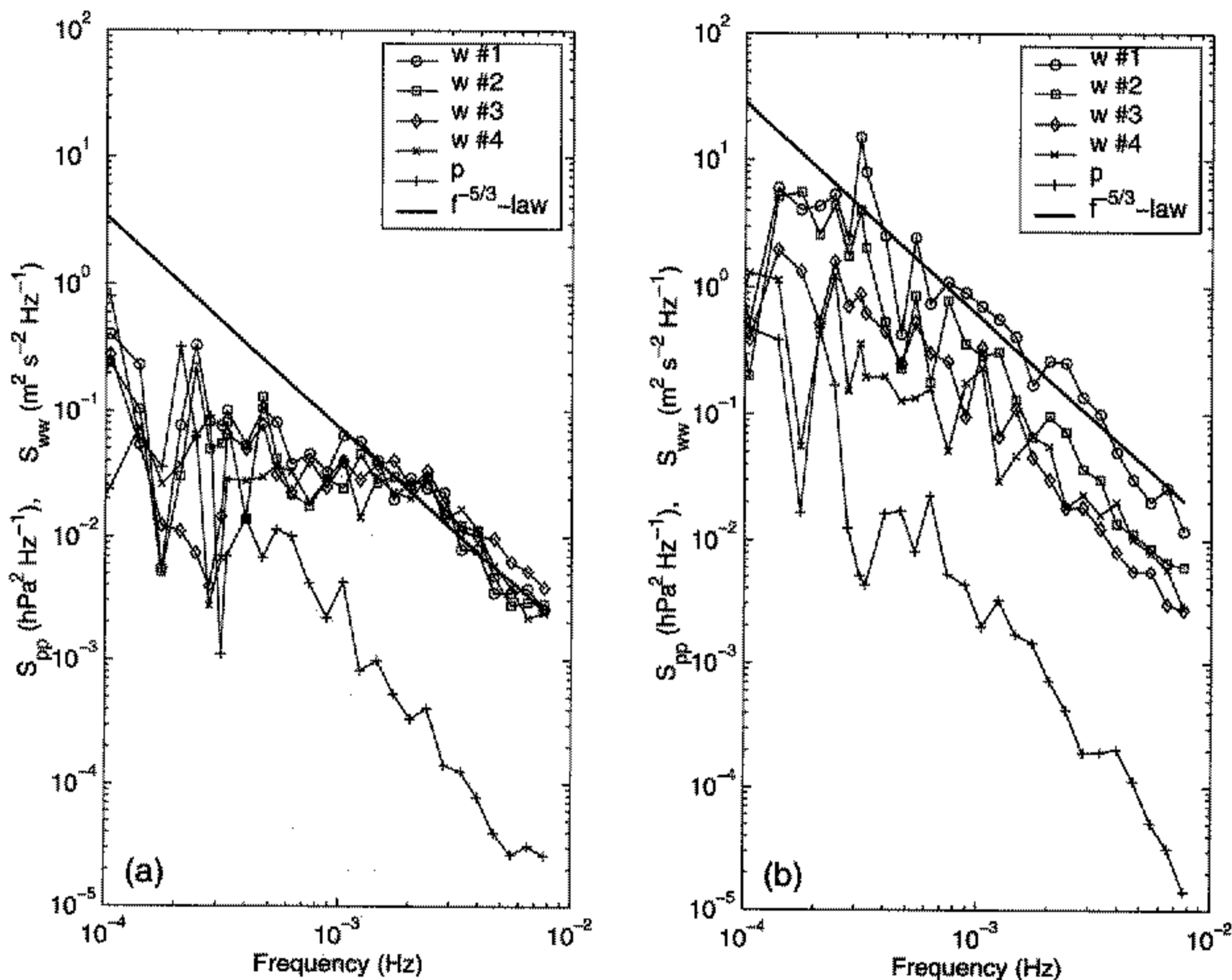


Figure 7. As Fig. 6, but with data from 26 May.

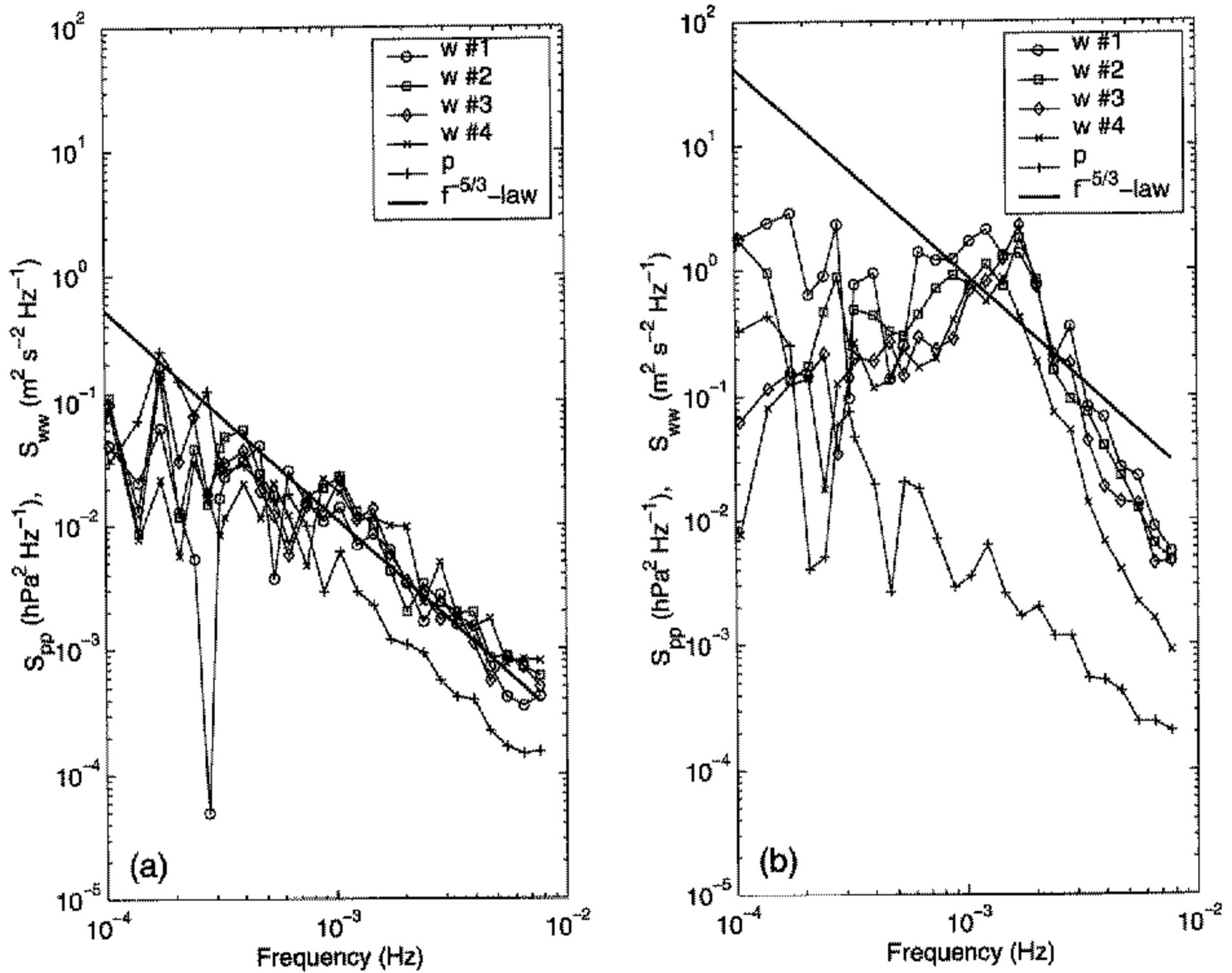


Figure 8. As Fig. 6, but with data from 27 May.

periods (0000–0800 UTC on 25, 26 and 27 May) and three 8 h long afternoon periods (1000–1800 UTC on 25, 26 and 27 May). Figures 6, 7 and 8 show  $S_{ww}(f)$  for the lowest four range gates and  $S_{pp}(f)$  during the morning and afternoon of 25 May (Fig. 6), 26 May (Fig. 7) and 27 May (Fig. 8); i.e. Figs. 6, 7 and 8 cover the lower troposphere. Vertical-velocity spectra at higher altitudes are shown in Figs. 9, 10 and 11.

#### (d) Diurnal cycle

As expected from the diurnal variation of the 1 h root-mean-square (r.m.s.) values of  $p$  at the surface and of  $w$  at the lowest radar range gate (Fig. 4), the levels of the  $w$  spectra also show a pronounced diurnal variation. In the lower troposphere (Figs. 6, 7 and 8) as well as in the middle and upper troposphere (Figs. 9, 10 and 11), the spectral levels of  $S_{ww}(f)$  are one or two orders of magnitude larger for the daytime period (1000–1800 UTC) than for the night-time period (0000–0800 UTC). In all six figures a  $-5/3$  power law is shown for orientation. The high-frequency parts of the 40 vertical-velocity spectra shown in Figs. 6–11 show a power law close to  $-5/3$ . Only the 27 May afternoon spectra (Figs. 8(b) and 11(b)) show a much steeper drop-off: the logarithmic slopes are between  $-3$  and  $-4$ . It is interesting that the slopes of the  $p$  spectra of 25 and 26 May (both night and day) are somewhat steeper than  $-5/3$ , while the slopes of the 27 May spectra (again both night and day) are very close to  $-5/3$ . That is, the steep drop-off on 27 May in the  $w$  spectra is not seen in the  $p$  spectra of that day.

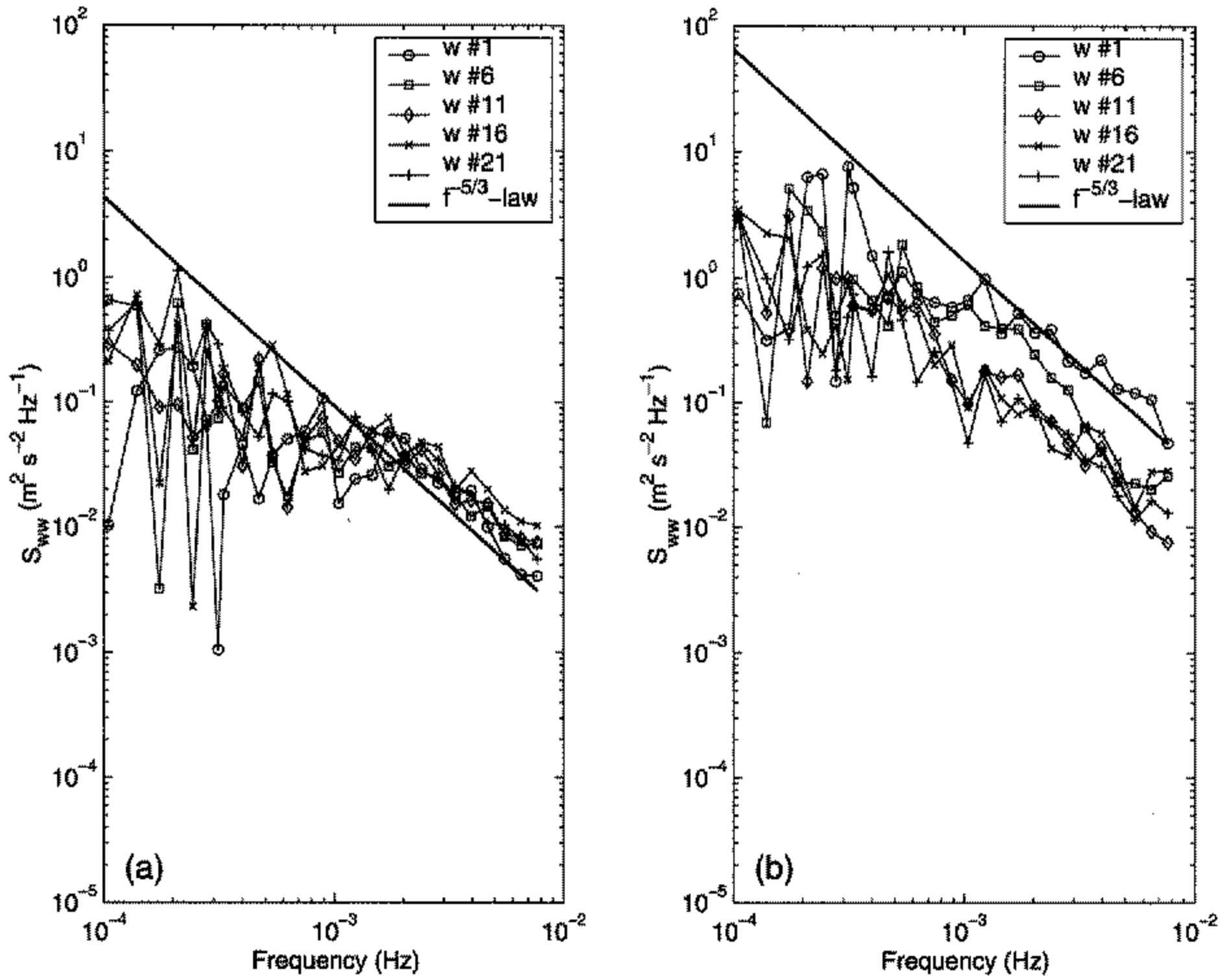


Figure 9. Frequency spectra of vertical velocity  $w$  at the five range gates 1, 6, 11, 16 and 21, which are centred at 2.7, 4.2, 5.7, 7.2 and 8.7 km, respectively, relative to mean sea level: (a) morning of 25 May 1999, and (b) afternoon of the same day. The  $-5/3$  power law is also shown.

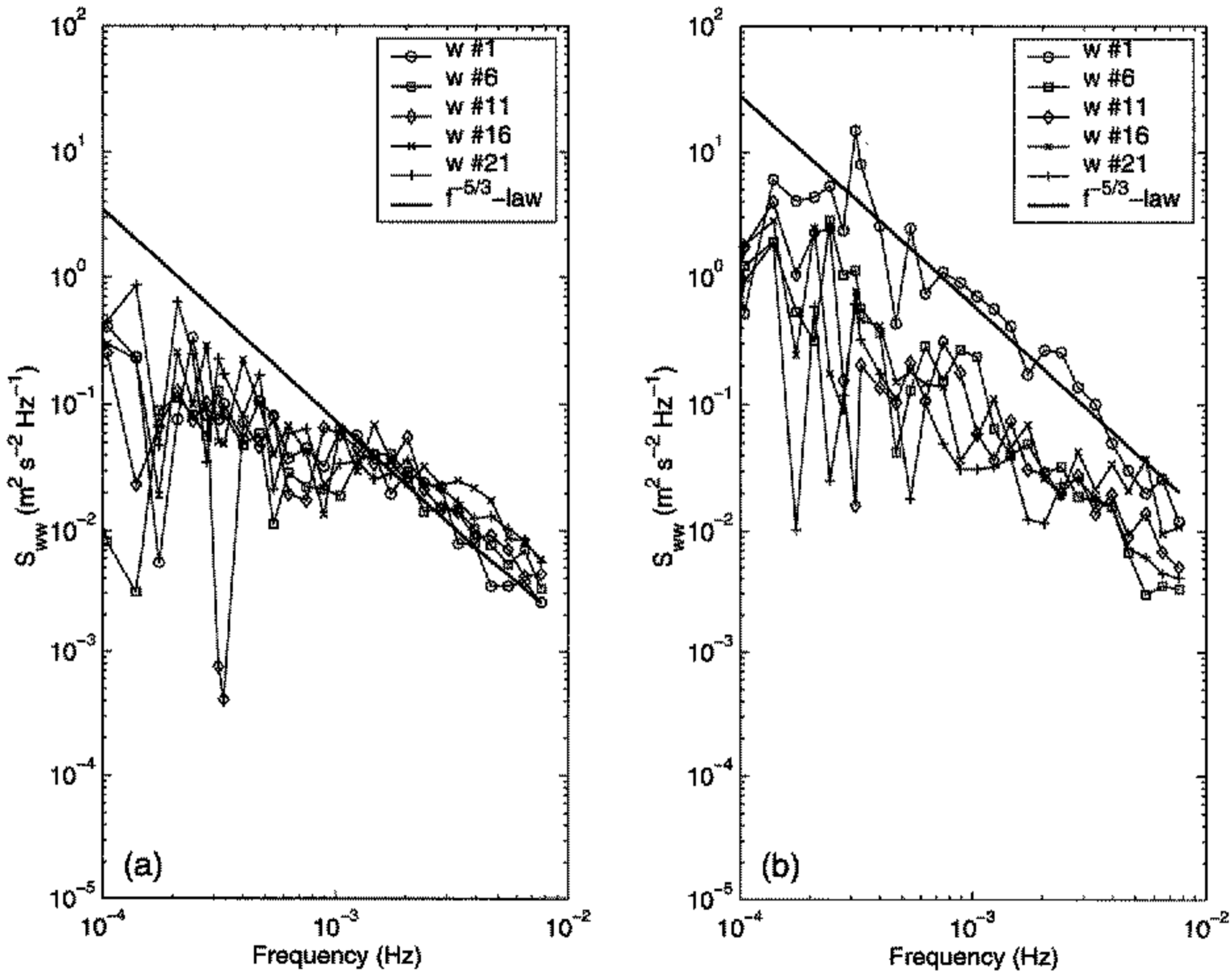


Figure 10. As Fig. 9, but with data from 26 May.

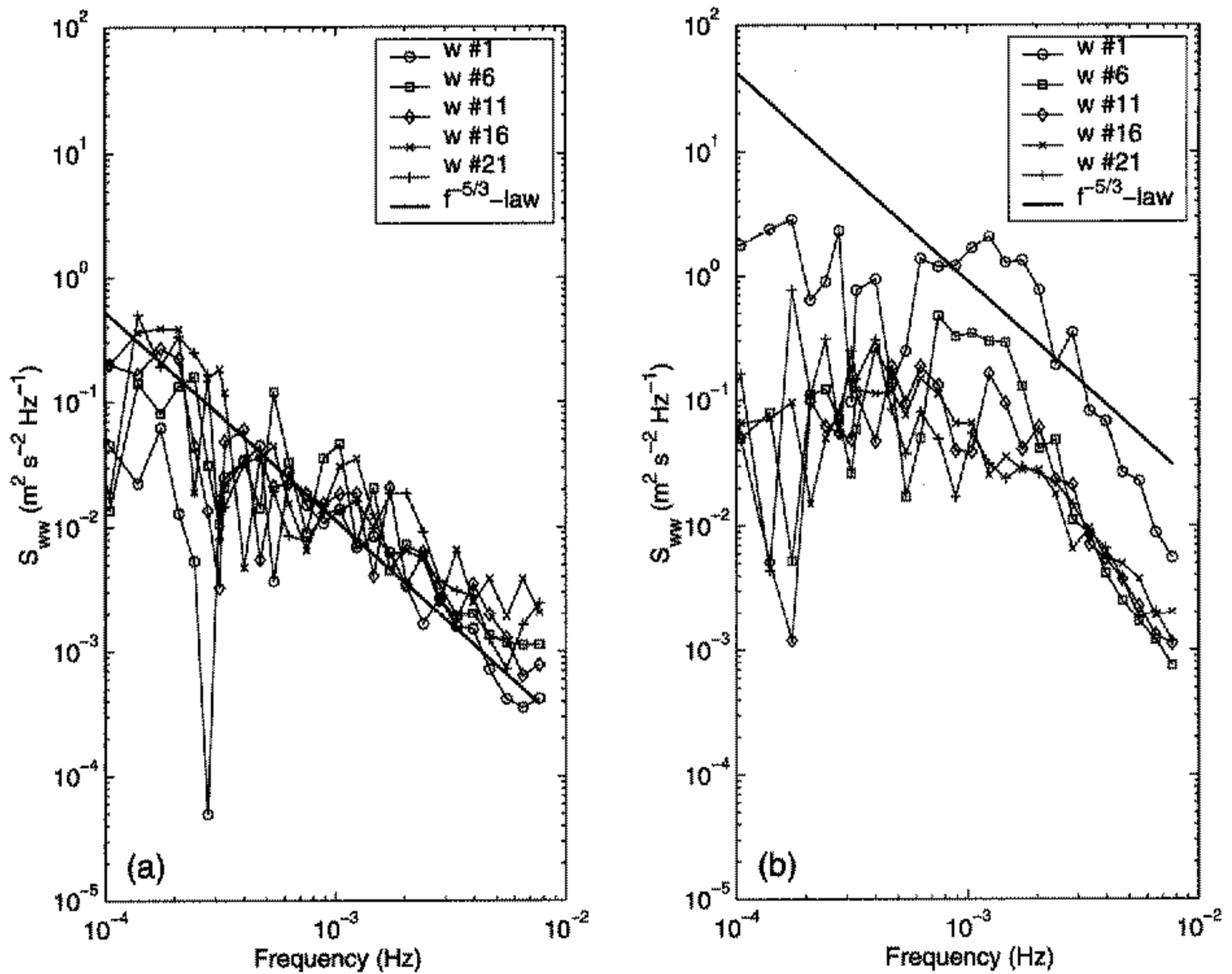


Figure 11. As Fig. 9, but with data from 27 May.

#### 4. DISCUSSION

##### (a) *Intrinsic (Lagrangian) and observed (Eulerian) gravity-wave spectra*

Before we discuss the observed spectra, we provide the essentials of how an intrinsic (Lagrangian), spatio-temporal gravity-wave spectrum  $L_{ww}(\omega_i, \mathbf{k})$  is mapped into a (Eulerian) frequency spectrum  $S_{ww}(\omega)$ . Consider the wave phase  $\varphi$  at time  $t$  and at a Lagrangian location  $\mathbf{x}_i$ :

$$\varphi = \omega_i t - \mathbf{k} \cdot \mathbf{x}_i, \tag{1}$$

where  $\omega_i$  is the intrinsic (Lagrangian) frequency of the gravity wave and  $\mathbf{k}$  is the horizontal wave vector. The Eulerian position  $\mathbf{x}$  is given by

$$\mathbf{x} = \mathbf{x}_i + \mathbf{V}t, \tag{2}$$

where  $\mathbf{V}$  is the mean horizontal velocity vector, i.e. the velocity vector of the Lagrangian coordinate system relative to the Eulerian coordinate system. Then the phase at time  $t$  and at the Eulerian position  $\mathbf{x}$  is given by

$$\varphi = \omega t - \mathbf{k} \cdot \mathbf{x}, \tag{3}$$

where the Eulerian frequency  $\omega$  turns out to be

$$\omega = \omega_i + \mathbf{k} \cdot \mathbf{V}. \tag{4}$$

The mapping from the intrinsic (Lagrangian) spectrum to the observed (Eulerian) spectrum can be written as follows, where the Dirac delta function in the integrand

handles the frequency mapping:

$$S_{ww}(\omega) = \int L_{ww}(\omega) \delta(\omega_i - \omega + \mathbf{k} \cdot \mathbf{V}) d\omega_i d^2k. \quad (5)$$

For a given  $\mathbf{k}$  and a given  $\mathbf{V}$  there is a frequency shift (Doppler shift) by the amount

$$\Delta\omega = \omega - \omega_i = \mathbf{k} \cdot \mathbf{V}. \quad (6)$$

The highest possible intrinsic frequency is the Brunt–Väisälä frequency,  $N = 2\pi/T_{BV}$ . Therefore, any energy in the observed spectrum that appears at a frequency  $\omega$  larger than  $N$  must have been Doppler-shifted by at least the amount  $\mathbf{k} \cdot \mathbf{V} = \omega - N$ . For a given  $\mathbf{V}$ , this determines the minimum wave number  $k_{\min}$  and the maximum wavelength  $\lambda_{\max} = 2\pi/k_{\min}$  at which spectral energy is seen in the Eulerian frequency spectrum at  $\omega$ :

$$\lambda_{\max} = 2\pi \frac{V}{\omega - N}. \quad (7)$$

That is, in the limit of  $\omega$  much larger than  $N$ , the maximum corresponding wavelength is obtained by a simple Taylor transformation. For the SOMARE-99 observations, the Nyquist frequency was  $\omega_{Ny} = 2\pi f_{Ny} = 2\pi/120 \text{ s}^{-1}$ , which was much larger than  $N$ . For a wind speed of  $10 \text{ m s}^{-1}$ , the maximum wavelength that appears at the SOMARE-99 Nyquist frequency is about 1.2 km.

Fritts and VanZandt (1987) begin their theoretical investigation of the mapping from Lagrangian to Eulerian gravity-wave spectra with the following simplified form of the Garrett and Munk (1975) model for the Lagrangian, horizontal-velocity spectrum:

$$L_{uu}(\omega_i, k) \propto \frac{\omega_i^{-p}}{k_* (1 + k/k_*)^t}, \quad (8)$$

where

$$k_* = \frac{\omega_i m_*}{N} = \frac{\omega_i}{c_i} \quad (9)$$

is a characteristic horizontal wave number ( $m_*$  is a characteristic vertical wave number, which Garrett and Munk (1975) and VanZandt (1982) assume to be independent of  $\omega_i$ );  $N = 2\pi/T_{BV}$  is the Brunt–Väisälä frequency;

$$c_i = \frac{N}{m_*} \quad (10)$$

is the characteristic horizontal phase speed;  $k$  is the magnitude of the horizontal wave vector  $\mathbf{k}$ ; and  $p$  and  $t$  are spectral exponents that are assumed to be quasi-universal.

On the basis of the simplified Garrett and Munk (1975) model, Eq. (8), Fritts and VanZandt (1987) derived a Lagrangian spectrum of vertical-velocity fluctuations. They used the equation for the Doppler shift, Eq. (4), to eliminate  $k$ , so that the Eulerian spectrum  $S_{ww}(\omega)$  could be written as an integral over a mixed Eulerian/Lagrangian frequency spectrum  $E_{ww}(\omega, \omega_i)$ :

$$S_{ww}(\omega) \propto \int E_{ww}(\omega, \omega_i) d\omega_i, \quad (11)$$

where (see Eq. (18) in Fritts and VanZandt (1987))

$$E_{ww}(\omega, \omega_i) \propto \frac{\omega_i^{t-1-p}}{\beta \omega_i \pm (\omega - \omega_i)/\cos \phi}. \quad (12)$$

Here  $\phi$  is the angle between  $\mathbf{V}$  and  $\mathbf{k}$ . The parameter  $\beta$  is the horizontal wind speed  $V$  normalized by  $c_1$ :

$$\beta = \frac{V}{c_1}. \quad (13)$$

Even without further analytically examining  $S_{ww}(\omega)$  here, it is obvious that the shape of  $S_{ww}(\omega)$  must depend on the scaled horizontal wind speed  $\beta$ . In their Fig. 4(b), Fritts and VanZandt (1987) show model results for  $S_{ww}(\omega)$  for various values of  $\beta$  from 0 to 10, assuming  $p = 2$  and  $t = 3$ . Their Fig. 4(b) is in qualitative agreement with the SOMARE-99 spectra: for low wind speeds ( $\beta$  smaller than 1),  $S_{ww}(\omega)$  cuts off steeply at  $\omega = N$ ; for higher wind speeds ( $\beta$  larger than 1), however, the logarithmic slope of  $S_{ww}(\omega)$  no longer changes suddenly. VanZandt *et al.* (1991) came to similar results and found reasonable agreement between  $S_{ww}(\omega)$  measured with the Flatland VHF radar and spectra simulated on the basis of the Garrett and Munk (1975) model, without neglecting the factor  $\{1 \pm (f_c/\omega)^2\}$ , where  $f_c$  is the Coriolis parameter.

#### (b) Interpretation of mean spectra

Fourier processing of a measured time series of fluctuations of a quantity  $q$  requires that the statistical characteristics of  $q$  are reasonably stationary during the observation period  $T$ . Only then does it make sense to consider the variance spectrum,  $S_{qq}(\omega)$ , as being representative for the period  $T$ .

Now consider a sequence of  $n$  observation periods  $T_i$  ( $i = 1, \dots, n$ ) and the corresponding sequence of  $n$  spectra  $S_{qq}^{(i)}(\omega)$ . Then the mean (incoherently averaged) spectrum is

$$\bar{S}_{qq}(\omega) = \frac{1}{n} \sum_{i=1}^n S_{qq}^{(i)}(\omega). \quad (14)$$

First we examine the mean of a sequence of turbulence spectra,

$$S_{qq}^{(i)}(\omega) = a_i \omega^{-5/3}, \quad (15)$$

where  $a_i$  is a sequence of spectral levels or turbulence structure parameters. Then the mean spectrum is

$$\bar{S}_{qq}(\omega) = \bar{a} \omega^{-5/3}, \quad (16)$$

where

$$\bar{a} = \frac{1}{n} \sum_{i=1}^n a_i. \quad (17)$$

That is, the structure parameter  $\bar{a}$  of the mean spectrum is equal to the mean of the individual structure parameters  $a_i$ .

Now consider a sequence of Eulerian gravity-wave spectra,

$$S_{qq}^{(i)}(\omega) = a_i \omega^{-b_i}. \quad (18)$$

In contrast to turbulence spectra, Eulerian gravity-wave spectra may have different logarithmic slopes  $b_i$ . (For the sake of simplicity, we assume here that the spectral slope is not a function of  $\omega$ .) Clearly, a power-law behaviour for  $\bar{S}_{qq}(\omega)$  in the general case cannot be expected a priori, and it is very difficult to interpret a gravity-wave spectrum obtained either by Fourier-processing a (statistically) non-stationary time series or by incoherently averaging over a sequence of spectra with different spectral slopes.

Consider the following instructive example: let  $a_i = \bar{a}$  be constant and the spectral slopes  $b_i$  be uniformly distributed between a certain  $b_1$ , which describes the flattest drop-off, to a  $b_2$  much larger than 1, corresponding to a slope associated with a sharp cut-off in the respective  $S_{qq}^{(i)}(\omega)$ . Then the mean spectrum is

$$\bar{S}_{qq}(\omega) = \frac{1}{b_2 - b_1} \int_{b_1}^{b_2} \bar{a} x^{-b} db = \frac{\bar{a}}{b_2 - b_1} \frac{(x^{-b_1} - x^{-b_2})}{\ln x}. \quad (19)$$

(Here we have used the normalized frequency  $x = \omega/N$ .) That is, the mean spectrum of an ensemble of spectra with (negative) slopes  $b$  uniformly distributed within an interval  $(b_1, b_2)$  behaves for  $x \gg 1$  like  $x^{-b_1}$ , where  $b_1$  is the flattest (least negative) slope. Since the flattest slopes in the high-frequency part of observed  $S_{ww}(f)$  are often close to  $-5/3$  (see Figs. 6, 7, 8(a), 9, 10 and 11(a); see also VanZandt *et al.* 1991), it is not surprising that the mean  $w$  spectra often vary like  $f^{-5/3}$  at high frequencies (e.g. Balsley and Carter 1982). The spectrum  $S_{ww}(f)$ , calculated for the entire 72 h period (Fig. 5), shows a high-frequency drop-off slightly steeper than  $f^{-5/3}$ , presumably because in this specific 72 h period there was a significant portion of 'quiet' periods with slopes steeper than  $-5/3$ .

We have seen that the logarithmic slope and the spectral level of Eulerian gravity-wave spectra can change dramatically within several hours. We suggest using the term *gravity-wave intermittency* for this non-stationary characteristic of gravity waves, analogous to the notion of turbulence intermittency (e.g. Kolmogorov 1962; Kuznetsov *et al.* 1992; Mahrt 1989). However, in contrast to turbulence intermittency, which is a small effect for many practical applications, gravity-wave intermittency appears to be a first-order effect for observation and simulation of atmospheric gravity waves.

### (c) Diurnal variation of gravity-wave activity

During the 72 h period that we analysed here, there was a pronounced diurnal cycle in all  $w$  spectra at all radar-observed altitudes between 2.7 and 8.7 km MSL. This diurnal cycle indicates that boundary-layer processes had a dominating effect on short-term vertical-velocity fluctuations (between 1 min and 1 h) throughout the troposphere. A diurnal cycle is also seen in the 1 h r.m.s.  $p$  values and in the  $p$  spectra (although not as pronounced as in the  $w$  spectra).

Bull (1985) presented an extensive climatology of gravity waves observed with a triangle of microbarographs on the island of Rügen in Northern Germany in the Baltic Sea. It is interesting that he observed a significant but very small diurnal cycle: the long-term averaged, 2 h r.m.s. value of  $p$  had an afternoon minimum and a morning maximum, but the difference between minimum and maximum amounted to only 15%. For the three days examined in the present study, however, we found an afternoon maximum and a night-time minimum of 1 h  $\sigma_p$ , the maximum exceeding the minimum by a factor of three or more. (The minimum values of  $\sigma_p$  shown in Fig. 4 are probably dominated by instrumental noise and therefore probably overestimate the real  $\sigma_p$  at those times.) Bull (1985) observed a mean 2 h  $\sigma_p$  of 3.3 Pa, which is comparable to the mean 1 h  $\sigma_p$  that we observed during SOMARE-99. A possible explanation for the strong diurnal cycle of the gravity-wave activity in the Harz Mountains and almost none

at Rügen is that Rügen is on the coast and the Harz Mountains are not. The air masses advected to Rügen are typically marine air masses with only little diurnal variability, whereas the air masses advected over the Harz Mountains are overland air masses strongly influenced by daytime heating and night-time cooling, particularly during anticyclonic periods like the SOMARE-99 period. In summary, the absence of a diurnal cycle of gravity-wave activity at Rügen is an additional indication for the relevance of boundary-layer processes for gravity waves in the troposphere over inland areas.

(d) *Gravity-wave generation mechanisms*

The strong diurnal cycle of the gravity-wave activity during SOMARE-99 indicates that boundary-layer convection was the dominating effect in generating the observed tropospheric gravity waves. In spite of the passage of the upper-level trough on 25 May around noon, it is interesting that the spectral levels of the 25 May  $w$  spectra in the middle and upper troposphere (Fig. 9(b)) are only a factor of two larger than the corresponding 26 May  $w$  spectra (Fig. 10(b)). The spectral levels of corresponding night-time spectra (Figs. 9(a) and 10(a)), however, are about an order of magnitude smaller than the daytime spectra and practically indistinguishable from each other. This may be seen as another indication for the dominating effect of boundary-layer convection.

Boundary-layer convection can lead to upward-propagating gravity waves through two mechanisms: first, when there is no geostrophic wind, convective elements (thermals, plumes) rise within the boundary layer, eventually hitting the capping inversion, and the perturbations of the capping inversion propagate upwards as gravity waves through the stably stratified, free troposphere (Deardorff *et al.* 1969). Second, when there is a moderate or strong geostrophic wind, the horizontal variability of the inversion height acts like a topography on the free troposphere aloft, leading to gravity waves similar to mountain waves (e.g. Hauf 1993, p. 3282). Clark *et al.* (1986) discuss the relative importance of these two mechanisms, i.e. 'thermal forcing' versus 'shear forcing'. Currently, we are not able to decide whether the different behaviours of the 27 May daytime spectra, as opposed to the 25 and 26 May daytime spectra, can be attributed to the different effects of convection under weak- and strong-wind conditions, respectively, or whether the difference in the spectra is a consequence of different values of the scaled horizontal wind  $\beta$ , as indicated in section 4(a).

Herron and Tolstoy (1969) provided observational evidence of a high correlation between the velocity vector of jet-stream winds and the velocity vector of surface-pressure disturbances observed with an array of microbarographs. This high correlation was confirmed by Neisser (1985) on the basis of observations using the Rügen microbarograph array. If the strong winds during the trough passage on 25 May had had a dominating effect on the upper-level gravity-wave activity, then we would expect that the difference between the spectra of 25 and 26 May would be greater than the night-time/daytime difference in the spectra of 25 and 26 May, respectively. However, because the trough passage on 25 May was nearly coincident with the maximum of convective activity (by coincidence), it is possible that the gravity-wave-generating effect of upper-level shear on 25 May was the same order of magnitude as the boundary-layer convection. Cross-spectral analysis of the data from all four microbarographs deployed during SOMARE-99 might clarify this issue.

(e) *How to distinguish between gravity waves and turbulence*

Whether the mesoscale variability in the atmosphere should be interpreted as gravity-wave activity or as turbulence has been discussed for several decades. For



obvious reasons, three-dimensional, Kolmogorov-type turbulence can be excluded for variability at length-scales larger than 1 km or so. (The only exception may be thunderstorms where isotropic turbulence at scales somewhat larger than 1 km is conceivable.) Nevertheless, two-dimensional turbulence (Kraichnan 1967) is a serious candidate for an alternative explanation.

In an important paper, Gage (1979) provided observational evidence for a  $f^{-5/3}$  power law in horizontal-wind-velocity variations observed with clear-air radar. On the basis of Taylor's hypothesis (which is questionable for gravity waves; see section 4(a)), he inferred a  $k^{-5/3}$  horizontal-wave-number spectrum for the mesoscale regime, and he interpreted it as evidence for two-dimensional turbulence. Later, aircraft measurements provided a  $k^{-5/3}$  power law directly, without relying on Taylor's hypothesis (Lilly and Petersen 1983; Nastrom and Gage 1983). Lilly (1983) discusses the relative importance of gravity-wave activity versus two-dimensional turbulence. He expects that the importance of both is comparable.

As we have pointed out in section 4(b), considering the mean spectra that result from averaging over large ensembles of individual spectra may not be the most appropriate approach. Possibly the key to distinguishing between gravity waves and two-dimensional turbulence lies in the short-term variability of the spectral characteristics. On the basis of the statistics of the parameters (spectral level, slope) of spectra computed from short (not more than several hours) time series, criteria for distinguishing the two might be developed, since it appears plausible that the intermittency statistics of gravity waves and the intermittency statistics of two-dimensional turbulence have little in common.

(f) *A peak in  $S_{ww}(f)$  at the Brunt–Väisälä frequency, and noise floor of  $S_{ww}(f)$*

It has been demonstrated that under favourable conditions the Brunt–Väisälä period can be retrieved from the radar-observed frequency spectra of vertical velocity (Röttger 1986; Revathy *et al.* 1996). Often, the Brunt–Väisälä frequency  $f_{BV} = 1/T_{BV}$  is marked as a peak in  $S_{ww}(f)$  when the horizontal wind is weak. Here we use this relationship between vertical temperature gradient (observed with radiosondes) and the radar-observed  $f_{BV}$  only as a consistency test: in the high-frequency part of  $S_{ww}(f)$  observed at the lowest range gate during the afternoon period of 27 May (Fig. 8(b), circles), there is a pronounced peak at  $f = 2.7 \times 10^{-3}$  Hz that corresponds to  $T_{BV} = 6.2$  min. Preliminary analysis of the vertical temperature gradients observed with radiosondes number 17, 18 and 19 (launched at 1200, 1500 and 1800 UTC, respectively) shows that  $T_{BV}$  was between 5 and 7 min at altitudes between the boundary-layer inversion and 5 km MSL.

Now, we estimate the  $w$  amplitude and the vertical-displacement amplitude of this Brunt–Väisälä oscillation. The spectral estimates shown in Fig. 8(b) are block averages over logarithmically equidistant frequency bins. The bin width is 1/14 decade, i.e. the relative bin width is  $10^{1/14} - 1 = 0.18$ . The absolute bin width at  $f = 2.7 \times 10^{-3}$  Hz is then  $\Delta f = 5 \times 10^{-4}$  Hz. Figure 8(b) shows that  $S_{ww}(f)$  is  $0.4 \text{ m}^2\text{s}^{-2}\text{Hz}^{-1}$  at the Brunt–Väisälä peak. Assuming that all the energy associated with the Brunt–Väisälä oscillation is concentrated in a single frequency bin of width  $\Delta f$ , we obtain a vertical-velocity variance  $\overline{w^2} = 2 \times 10^{-4} \text{ m}^2\text{s}^{-2}$ . Assuming that  $w$  varies sinusoidally with time, the square of the vertical-velocity amplitude is  $w_0^2 = 2\overline{w^2}$ , and we obtain  $w_0 = 2 \text{ cm s}^{-1}$ . Given  $w_0$  and  $N$ , we obtain the vertical-displacement amplitude

$$z_0 = \int_0^{\pi/2} w_0 \cos(Nt) dt = \frac{w_0}{N}. \quad (20)$$

With  $N = 2\pi/(6 \text{ min})$  and  $w_0 = 2 \text{ cm s}^{-1}$ , we obtain  $z_0 = 1.1 \text{ m}$ . Obviously both  $w_0$  and  $z_0$  are very small.

The low noise floor in the  $w$  spectra is remarkable: up to the Nyquist frequency, none of the  $w$  spectra (Figs. 5–11) shows a flattening due to uncorrelated noise. The noise floor is  $10^{-3} \text{ m}^2\text{s}^{-1}\text{Hz}^{-1}$  or less. That is, the standard deviation of uncorrelated noise in the 1 min  $w$  samples is  $3 \text{ mm s}^{-1}$  or less.

We arrive at the same value for the noise floor as follows: the width of a velocity bin in the raw spectrum is  $\Delta w = \lambda/(2T_d)$ , where  $T_d$  (1 min in our case) is the dwell time (see Gossard and Strauch 1983, Eqs. (11–10)). The noise floor  $S_d$  for digitization noise over the band width  $f_{\text{Ny}}$  is given by  $S_d f_{\text{Ny}} = \Delta w^2/12$ . The noise floor is further reduced by the factor  $n_f n_p$ , where  $n_f$  is the number of carrier frequencies (which ideally provide independent  $w$  samples), in our case four, and  $n_p$  is the number of spectral points that contribute significantly to the ‘wind peak’ in the Doppler spectrum. That is, the theoretical value of the resulting noise floor is

$$S_n = \frac{1}{12n_f n_p} \left( \frac{\lambda}{2T_d} \right)^2 \frac{1}{f_{\text{Ny}}}. \quad (21)$$

For  $\lambda = 6 \text{ m}$  and  $n_p = 25$ , we obtain  $S_n = 10^{-3} \text{ m}^2\text{s}^{-1}\text{Hz}^{-1}$ , which is the noise floor value that we estimated from the observed spectra.

## 5. SUMMARY AND CONCLUSIONS

Vertical-velocity fluctuations in the free troposphere and surface-pressure fluctuations were observed during the 72 h period between 0000 UTC 25 May and 0000 UTC 28 May by using the SOUSY VHF radar and a microbarograph, respectively. A pronounced diurnal cycle was observed in the 1 h standard deviations as well as in the frequency spectra of both  $w$  (at altitudes from 2.7 and 8.7 km MSL) and  $p$ , indicating the relevance of boundary-layer convection for short-term  $w$  fluctuations throughout the troposphere above the Harz mountains in Northern Germany.

Previous work on  $w$  fluctuations observed with vertically oriented radar wind profilers and mesospheric–stratospheric–tropospheric (MST) radars has predominantly been focused on the effect of orography, probably for historical reasons: while mountain waves with  $w$  amplitudes of up to several meters per second and time-scales of several hours are seen immediately in height–time sections of  $w$  observed with vertically oriented wind profilers or MST radars, it is technically much more demanding to observe Eulerian, Doppler-shifted gravity-wave  $w$  spectra under fair-weather conditions where  $w$  amplitudes are typically much smaller (as small as  $1 \text{ cm s}^{-1}$ ) and have much shorter time-scales (down to 1 min or even less), as we have demonstrated in this paper.

One purpose of this paper has been to shift the apparently selective attention of the wind-profiler and MST-radar community away from the orographic effects on gravity waves and towards the effects of boundary-layer convection. The relevance of boundary-layer convection on tropospheric gravity waves has been fairly convincingly demonstrated by the mesoscale meteorology community on the basis of simulations and aircraft measurements (e.g. Clark *et al.* 1986; Kuettner *et al.* 1987; Hauf and Clark 1989; Hauf 1993). Further research, however, taking full advantage of the superior height/time coverage capabilities of radar wind profilers, could lead to a more quantitative determination of the relative importance of boundary-layer convection (as opposed to other phenomena, like jet-stream passages, frontal passages, or flow over mountainous terrain) for the generation of gravity waves, parametric in time of day, time of year, altitude, horizontal wind speed, geographic location (coastal versus inland), and so on.

## ACKNOWLEDGEMENTS

SOMARE-99 was jointly supported by the Max Planck Institute for Aeronomy, Katlenburg-Lindau, Germany; the National Oceanic and Atmospheric Administration's Environmental Technology Laboratory, Boulder, Colorado; the Swedish Institute of Space Physics, Kiruna, Sweden; the German Weather Service, Offenbach, Germany; and the German Weather Service's Meteorological Observatory Lindenberg, Lindenberg, Germany.

## REFERENCES

- Balsley, B. B. and Carter, D. A. 1982 The spectrum of atmospheric velocity fluctuations at 8 km and 86 km. *Geophys. Res. Lett.*, **9**, 465–468
- 1989 Mountain waves in the tropical Pacific atmosphere: A comparison of vertical wind fluctuations over Pohnpei and Christmas Island using VHF wind profilers. *J. Atmos. Sci.*, **46**, 2698–2715
- Batchelor, G. K. 1953 *The theory of homogeneous turbulence*. Cambridge University Press
- Brunt, M. A. 1927 The period of simple vertical oscillations in the atmosphere. *Q. J. R. Meteorol. Soc.*, **53**, 30–32
- Bull, G. 1985 A study of statistical properties of atmospheric gravity waves. *Z. Meteorol.*, **35**, 73–83
- Chilson, P. B. and Schmidt, G. 1996 Implementation of frequency domain interferometry at the SOUSY VHF Radar: First results. *Radio Sci.*, **31**, 263–272
- Chilson, P. B., Muschinski, A. and Schmidt, G. 1997 First observations of Kelvin–Helmholtz billows in an upper-level jet stream using VHF frequency domain interferometry. *Radio Sci.*, **32**, 1149–1160
- Chilson, P. B., Palmer, R. D., Muschinski, A., Hooper, D. A., Schmidt, G. and Steinhagen, H. 2001 SOMARE-99: A demonstrational field campaign for ultra-high-resolution VHF atmospheric profiling using frequency diversity. *Radio Sci.* (in press)
- Clark, T. L., Hauf, T. and Kuettner, J. P. 1986 Convectively forced internal gravity waves: Results from two-dimensional numerical experiments. *Q. J. R. Meteorol. Soc.*, **112**, 899–925
- Deardorff, J. W., Willis, E. E. and Lilly, D. K. 1969 Laboratory investigation of non-steady penetrative convection. *J. Fluid Mech.*, **35**, 7–31
- Ecklund, W. L., Balsley, B. B., Carter, D. A., Riddle, A. C., Crochet, M. and Gerello, R. 1985 Observations of vertical motions in the troposphere and lower stratosphere using three closely spaced ST radars. *Radio Sci.*, **20**, 1196–1206
- Einaudi, F., Lalas, D. P. and Perona, G. E. 1979 The role of gravity waves in tropospheric processes. *Pure Appl. Geophys.*, **117**, 627–663
- Fritts, D. C. and VanZandt, T. E. 1987 Effects of Doppler shifting on the frequency spectra of atmospheric gravity waves. *J. Geophys. Res.*, **92**, 9723–9732
- Gage, K. S. 1979 Evidence for a  $k^{-5/3}$  law inertial range in mesoscale two-dimensional turbulence. *J. Atmos. Sci.*, **36**, 1950–1954
- Garrett, C. and Munk, W. 1972 Space–time scales of internal waves. *Geophys. Fluid Dyn.*, **2**, 225–264
- 1975 Space–time scales of internal waves: A progress report. *J. Geophys. Res.*, **80**, 291–297
- Gossard, E. E. 1962 Vertical flux of energy into the lower ionosphere from internal gravity waves generated in the troposphere. *J. Geophys. Res.*, **67**, 745–757
- Gossard, E. E. and Hooke, W. H. 1975 *Waves in the atmosphere*. Elsevier, Amsterdam, The Netherlands
- Gossard, E. E. and Strauch, R. G. 1983 *Radar observations of clear air and clouds*. Elsevier, Amsterdam, The Netherlands
- Hauf, T. 1993 Aircraft observation of convection waves over Southern Germany—a case study. *Mon. Weather Rev.*, **121**, 3282–3290
- Hauf, T. and Clark, T. L. 1989 Three-dimensional numerical experiments on convectively forced internal gravity waves. *Q. J. R. Meteorol. Soc.*, **115**, 309–333
- Herron, T. and Tolstoy, I. 1969 Tracking jet stream winds from ground level pressure signals. *J. Atmos. Sci.*, **26**, 266–269
- Hines, C. O. 1960 Internal gravity waves at ionospheric heights. *Canad. J. Phys.*, **38**, 1441–1481

- Hines, C. O. 1989 Tropopausal mountain waves over Arecibo: A case study. *J. Atmos. Sci.*, **46**, 476–488
- Hines, C. O. and Reddy, C. A. 1967 On the propagation of atmospheric gravity waves through regions of wind shear. *J. Geophys. Res.*, **72**, 1015–1034
- Kaimal, J. C. 1986 Flux profile measurements from towers in the boundary layer. Pp. 19–28 in *Probing the atmospheric boundary layer*. Ed. D. H. Lenschow. American Meteorological Society, Boston, USA
- Kaimal, J. C., Wyngaard, J. C., Izumi, Y. and Coté, O. R. 1972 Spectral characteristics of surface-layer turbulence. *Q. J. R. Meteorol. Soc.*, **98**, 563–589
- Kaimal, J. C., Wyngaard, J. C., Haugen, D. A., Coté, O. R. and Izumi, Y. 1976 Turbulence structure in the convective boundary layer. *J. Atmos. Sci.*, **33**, 2152–2169
- Kolmogorov, A. N. 1941 Energy dissipation in locally isotropic turbulence. *Dokl. Akad. Nauk SSSR*, **30**, 299–303
- 1962 A refinement of previous hypotheses concerning the local structure of turbulence in a viscous incompressible fluid at high Reynolds number. *J. Fluid Mech.*, **13**, 82–85
- Kraichnan, R. H. 1967 Inertial ranges in two-dimensional turbulence. *Phys. Fluids*, **10**, 1417–1423
- Kudeki, E. and Stitt, G. 1987 Frequency domain interferometry: A high resolution radar technique for studies of atmospheric turbulence. *Geophys. Res. Lett.*, **14**, 198–201
- Kuettner, J. P., Hildebrand, P. A. and Clark, T. L. 1987 Convection waves: Observations of gravity wave systems over convectively active boundary layers. *Q. J. R. Meteorol. Soc.*, **113**, 445–467
- Kuznetsov, V. R., Praskovsky, A. A. and Sabelnikov, V. A. 1992 Fine-scale turbulence structure of intermittent shear flows. *J. Fluid Mech.*, **243**, 595–622
- Lilly, D. K. 1971 Observations of mountain-induced turbulence. *J. Geophys. Res.*, **76**, 6585–6588
- 1983 Stratified turbulence and the mesoscale variability of the atmosphere. *J. Atmos. Sci.*, **40**, 749–761
- Lilly, D. K. and Petersen, E. L. 1983 Aircraft measurements of atmospheric kinetic energy spectra. *Tellus*, **35A**, 379–382
- Lindzen, R. S. 1981 Turbulence and stress owing to gravity wave and tidal breakdown. *J. Geophys. Res.*, **86**, 9707–9721
- Luce, H., Yamamoto, M., Fukao, S., Helal, D. and Crochet, M. 2001 A frequency domain radar interferometric imaging (FII) technique based on high-resolution methods. *J. Atmos. Solar-Terr. Phys.*, **63**, 221–234
- Lumley, J. L. and Panofsky, H. A. 1964 *The structure of atmospheric turbulence*. Wiley, New York, USA
- Mahrt, L. 1989 Intermittency of atmospheric turbulence. *J. Atmos. Sci.*, **46**, 79–95
- Monin, A. S. and Obukhov, A. M. 1953 Dimensionless characteristics of turbulence in the atmospheric surface layer. *Dokl. Akad. Nauk SSSR*, **93**, 223–226
- 1954 Basic turbulent mixing laws in the atmospheric surface layer. *Trudy Geofiz. Inst. Akad. Nauk SSSR*, **24**, 163–187
- Muschinski, A., Chilson, P. B., Kern, S., Nielinger, J., Schmidt, G. and Prenosil, T. 1999a First frequency-domain interferometry observations of large-scale vertical motion in the atmosphere. *J. Atmos. Sci.*, **56**, 1248–1257
- Muschinski, A., Sullivan, P. P., Wuertz, D. B., Hill, R. J., Cohn, S. A., Lenschow, D. H. and Doviak, R. J. 1999b First synthesis of wind profiler signals on the basis of Large-Eddy Simulation data. *Radio Sci.*, **34**, 1437–1459
- Nastrom, G. D. and Gage, K. S. 1983 A first look at wavenumber spectra from GASP data. *Tellus*, **35A**, 383–388
- 1984 A brief climatology of vertical wind variability in the troposphere and stratosphere as seen by the Poker Flat, Alaska, MST radar. *J. Clim. Appl. Meteorol.*, **23**, 453–460
- Nastrom, G. D., Ecklund, W. L., Gage, K. S. and Strauch, R. G. 1985 The diurnal cycle of backscattered power from VHF Doppler radar measurements in Colorado and Alaska. *Radio Sci.*, **20**, 1509–1517
- Neisser, J. 1985 Über den Zusammenhang zwischen atmosphärischen Schwerkwellen und hochtroposphärischen Strahlströmen. *Z. Meteorol.*, **35**, 257–266
- Obukhov, A. M. 1960 Structure of temperature and velocity fields under conditions of free convection. *Izv. Akad. Nauk SSSR Ser. Geofiz.*, **9**, 1392–1396
- Palmer, R. D., Yu, T.-Y. and Chilson, P. B. 1999 Range imaging using frequency diversity. *Radio Sci.*, **34**, 1485–1496

- Palmer, R. D., Chilson, P. B., Muschinski, A., Schmidt, G., Yu, T.-Y. and Steinhagen, H. 2001 SOMARE-99: Observations of tropospheric scattering layers using range imaging. *Radio Sci.* (in press)
- Ralph, F. M., Crochet, M. and Venkateswaran, S. V. 1992 A study of mountain lee waves using clear-air radar. *Q. J. R. Meteorol. Soc.*, **118**, 597–627
- Ralph, F. M., Neimann, P. J., Keller, T. L., Levinson, D. and Fedor, L. 1997 Observations, simulations, and analysis of nonstationary trapped lee waves. *J. Atmos. Sci.*, **54**, 1308–1333
- Revathy, K., Prabhakaran Nair, S. R. and Krishna Murty, B. V. 1996 Deduction of temperature profile from MST radar observations of vertical wind. *Geophys. Res. Lett.*, **23**, 285–288
- Röttger, J. 1986 Determination of Brunt–Väisälä frequency from vertical velocity spectra. *MAP Handb.*, **20**, 168–172
- Scorer, R. S. 1949 Theory of waves in the lee of mountains. *Q. J. R. Meteorol. Soc.*, **75**, 41–56
- Sheffler, A. O. and Liu, C. H. 1985 On observation of gravity wave spectra in the atmosphere by using MST radars. *Radio Sci.*, **20**, 1309–1322
- 1986 The effects of Doppler shift on gravity wave spectra observed by MST radar. *J. Atmos. Terr. Phys.*, **48**, 1225–1231
- Taylor, G. I. 1938 The spectrum of turbulence. *Proc. R. Soc. London*, **A164**, 476–490
- Townsend, A. A. 1966 Internal waves produced by a convective layer. *J. Fluid Mech.*, **24**, 307–319
- VanZandt, T. E. 1982 A universal spectrum of buoyancy waves in the atmosphere. *Geophys. Res. Lett.*, **9**, 575–578
- VanZandt, T. E., Nastrom, G. D. and Green, J. L. 1991 Frequency spectra of vertical velocity from Flatland VHF radar data. *J. Geophys. Res.*, **96**, 2845–2855
- Worthington, R. M. 1998 Tropopause turbulence caused by the breaking of mountain waves. *J. Atmos. Solar-Terr. Phys.*, **60**, 1543–1547
- Worthington, R. M. and Thomas, L. 1996 Radar measurements of critical-layer absorption in mountain waves. *Q. J. R. Meteorol. Soc.*, **122**, 1263–1282
- Worthington, R. M., Muschinski, A. and Balsley, B. B. 2001 Bias in mean vertical wind measured by VHF radars: Significance of radar location relative to mountains. *J. Atmos. Sci.* (in press)
- Zhou, J., Sud, Y. C. and Lau, K.-M. 1996 Impact of orographically induced gravity-wave drag in the GLA GCM. *Q. J. R. Meteorol. Soc.*, **122**, 903–927